Opt Quant Electron (2016) 48:556
DOI 10.1007/s11082-016-0823-4

Optical properties of a four-layer waveguiding nanocomposite structure in near-IR regime

I. S. Panyaev[1] · N. N. Dadoenkova[1,2] · Yu S. Dadoenkova[1,2,3] · I. A. Rozhleys[4] · M. Krawczyk[5] · I. L. Lyubchanskii[2] · D. G. Sannikov[1]

Received: 17 August 2016 / Accepted: 17 November 2016 / Published online: 28 November 2016

Abstract We present a theoretical study of the optical properties of TE- and TM- modes in a four-layer structure composed of a magneto-optical yttrium iron garnet guiding layer on a dielectric non-magnetic substrate covered by a planar nanocomposite guiding multilayer. We examine important issues for TM-modes, calculate and compare in details the dispersion spectra and the energy flux distributions across the structure for TE- and TM-modes of different orders and show new features concerning the splitting, switching and filtration possibilities of the fundamental modes of the orthogonal polarizations. The presented theoretical approach may be utilized for designing of different magneto-optical devices with preselected optical properties.

Keywords Nanocomposite · Magneto-optical · Optical waveguide · Long-wave approximation

This article is part of the Topical Collection on Optical Wave and Waveguide Theory and Numerical Modelling 2016.

Guest edited by Krzysztof Anders, Xuesong Meng, Gregory Morozov, Sendy Phang, and Mariusz Zdanowicz.

✉ D. G. Sannikov
sannikov-dg@yandex.ru

[1] Ulyanovsk State University, Ulyanovsk, Russian Federation 432017

[2] Donetsk Physical and Technical Institute of the National Academy of Sciences of Ukraine, Donetsk 83114, Ukraine

[3] Novgorod State University, Veliky Novgorod, Russian Federation 173003

[4] National Research Nuclear University MEPhI, Moscow, Russian Federation 115409

[5] Faculty of Physics, Adam Mickiewicz University in Poznań, 61–614 Poznan, Poland

1 Introduction

The investigations of the optical four-layer structures have began with the early theoretical works on isotropic waveguides (Tien et al. 1969; Tien and Ulrich 1970; Tien et al. 1972). The early experimental measurements of the waveguide modal characteristics have been carried out by Tien et al. (1973) and Sun and Muller (1977). The four-layer structures have been used, for example, in the polarizers of TE- and TM-modes (Polky and Mitchell 1974), leaky modes lasers (Scifres et al. 1976), optical waveguide lenses and tapered couplers (Southwell 1977), mode filters (Kudo and Mushiake 1982), thin-film Luneburg lens (Hewak and Lit 1987; Tabib-Azar 1995), mid-infrared modulators and switches (Stiens et al. 1994, 1997), etc. Apart from that, the advantages of a four-layer waveguide structure in comparison with a three-layer one are the more versatile possibilities of a light control within it. On the other hand, stratified structures consisting of five and more layers require more complex mathematical analysis which does not always give the complete clarity.

Multilayered nanocomposite (NC) structures are of great interest due to their specific properties. Such structures based on films with thicknesses of a few tens of nanometers are successfully used for electronic and photonic applications (Haus 2016). During the last decade different multilayered waveguide structures have been studied: magnetic photonic crystals (Khokhlov et al. 2015; Khosravi et al. 2015; Sylgacheva et al. 2016a, b), multilayered waveguides (Dotsch et al. 2005), silicon-based hybrid gap surface plasmon polariton waveguides (Rao and Tang 2012), nanophotonic and plasmonic waveguides (Alaeian and Dionne 2014) and multilayer graphene waveguides (Smirnova et al. 2014). Despite the considerable number of publications in this area, the NC waveguide structures still remain outside of research.

The dispersion and energy properties of the eigenwaves in a four-layer structure composed of a magneto-optical (MO) yttrium-iron garnet (YIG) waveguiding layer on a dielectric substrate covered by a planar NC guiding multilayer have been recently studied by Panyaev et al. (2016). The main results presented in this paper are the dispersion equation for the considered four-layer structure and the original algorithm for the guided modes identification. Nevertheless, the research was focused on the propagation and energetic properties of the guided TE-modes. In the present paper, we develop our investigation and in addition to our previous study we examine important issues for TM-modes, calculate and compare in details the dispersion spectra, as well as the energy flux distributions across the structure for orthogonally polarized modes of different orders. Moreover, we show new features concerning the power filtration and splitting of the fundamental TE and TM modes. The structure is described in terms of the effective medium approach (Agranovich and Kravtsov 1985; Brekhovskikh 1980; Rytov 1956) which allows to identify the guided modes and to obtain their electric and magnetic fields distributions across the structure. The concept of the limits for the nanolayer thicknesses in the NC is also discussed.

2 Theoretical analysis

The four-layer waveguide structure consists of a thick SiO_2 substrate, a MO film of YIG with the thickness L_1, covered by the one-dimensional NC multilayer of the thickness L_2 and an air playing the role of a cladding (as shown in Fig. 1). The NC multilayer with the period $d = d_{GGG} + d_{TiO_2}$ is formed by alternating nanolayers of gadolinium-gallium garnet

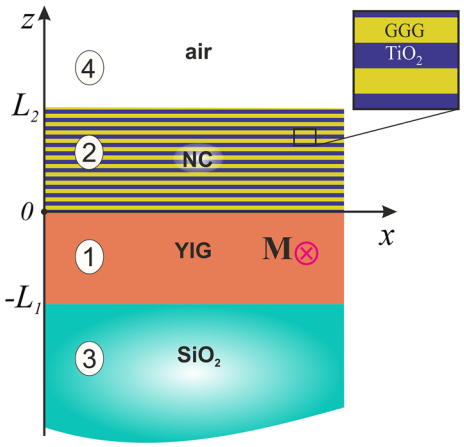

Fig. 1 Schematic of the guiding structure: YIG (layer 1); NC multilayer (layer 2); SiO_2 substrate (layer 3); air (layer 4)

(GGG) $Gd_3Ga_5O_{12}$ and titanium dioxide TiO_2 with the thicknesses d_{GGG} and d_{TiO_2}, respectively. We consider the transverse MO configuration, so the electromagnetic wave propagates along the x-axis, and the magnetization vector **M** is perpendicular to the wave propagation direction and oriented in-plane along the y-axis. In this case the electromagnetic eigenwaves in the YIG layer split into independent TE- and TM-modes (Zvezdin and Kotov 1997).

It is well known that YIG is transparent in the near IR regime (Randoshkin and Chervonenkis 1990; Zvezdin and Kotov 1997) and exhibits bigyrotropic properties, so both dielectric permittivity $\hat{\varepsilon}_{YIG}$ and magnetic permeability $\hat{\mu}_{YIG}$ tensors contain nonzero off-diagonal components. In the linear MO approximation, for **M** directed along the y-axis, the permittivity and permeability tensors have the following form (Gurevich and Melkov 1996):

$$\hat{\varepsilon}_{YIG} = \begin{pmatrix} \varepsilon_1 & 0 & i\varepsilon_a \\ 0 & \varepsilon_1 & 0 \\ -i\varepsilon_a & 0 & \varepsilon_1 \end{pmatrix}, \quad \hat{\mu}_{YIG} = \begin{pmatrix} \mu_1 & 0 & i\mu_a \\ 0 & \mu_1 & 0 \\ -i\mu_a & 0 & \mu_1 \end{pmatrix}. \tag{1}$$

The permittivity tensors of the materials, constituting the NC (based on GGG and TiO_2 nanolayers) are diagonal: $\hat{\varepsilon}_{GGG} = \varepsilon_{GGG}\hat{I}$ and $\hat{\varepsilon}_{TiO_2} = \varepsilon_{TiO_2}\hat{I}$, where $\hat{I} = \delta_{ik}$, and δ_{ik} is the Kronecker's delta. We assume the electromagnetic field changes weakly at the distances of about the wavelength λ of the electromagnetic wave, so the d_{GGG}, $d_{TiO_2} \ll \lambda$, and $d_N \ll L_{1,2}$, where $d_N = \max(d_{GGG}, d_{TiO_2})$. Moreover, for each nanolayer ξ the following inequality should be satisfied: $h\,d_\xi \ll 1$ (here h is a transverse wave vector component in a guiding layer) (Agranovich and Kravtsov 1985; Rytov 1956). Thus the long-wave approximation can be used, so the NC permittivity has the form (Agranovich and Kravtsov 1985):

$$\hat{\varepsilon}_{NC} = \begin{pmatrix} \varepsilon_{xx} & 0 & 0 \\ 0 & \varepsilon_{yy} & 0 \\ 0 & 0 & \varepsilon_{zz} \end{pmatrix}, \quad \varepsilon_{xx} = \varepsilon_{yy} = \frac{\Theta\varepsilon_{GGG} + \varepsilon_{TiO_2}}{\Theta + 1}, \quad \varepsilon_{zz} = \frac{\varepsilon_{GGG}\varepsilon_{TiO_2}(\Theta + 1)}{\Theta\varepsilon_{TiO_2} + \varepsilon_{GGG}}, \tag{2}$$

where $\Theta = d_{GGG}/d_{TiO_2}$ is the ratio of the GGG and TiO_2 layers thicknesses.

The substrate (SiO_2) and the cladding (air) have the scalar permittivities ε_3 and ε_4, respectively. In the considered frequency range (the near IR regime) the permeabilities of each layer are equal to unity, i.e. $\mu_1 = \mu_2 = \mu_3 = \mu_4 = 1$.

The electric and magnetic fields of the electromagnetic wave of the angular frequency ω, propagating along the x-axis, are proportional to $\exp[i(\omega t - \beta x)]$, where β is the propagation constant. The tangential components of the profile function $F(z)$ (the electric field component E_y for TE-mode and the magnetic field component H_y for TM-mode) have the following form:

$$F(z) = A \cdot \begin{cases} \cos h_1 z + C_1 \sin h_1 z, & -L_1 \le z \le 0, \\ \cos h_2 z + C_2 \sin h_2 z, & 0 \le z \le L_2, \\ [\cos h_1 L_1 - C_1 \sin h_1 L_1] e^{p(z+L_1)}, & z \le -L_1, \\ [\cos h_2 L_2 + C_2 \sin h_2 L_2] e^{-q(z-L_2)}, & z \ge L_2. \end{cases} \tag{3}$$

According to Yariv and Yeh (2007), we choose a suitable value of the arbitrary constant A which is useful for the further analysis. Namely, here A is the normalized amplitude which can be calculated by integrating the longitudinal component of the Poynting vector's. As a rule, the normalization procedure is important only for the excitation problems (Manenkov 1981), which are not the topic of this research. Assuming the value of the power per unit length along the y-axis to be of the order of 1 W/m (Yariv and Yeh 1984), we obtain the value of the normalized amplitude A in Eq. (3) using the expression $A^2 = 8\pi/(c \int_{-\infty}^{\infty} E_y H_z dz)$ for TE-modes and $A^2 = -8\pi/(c \int_{-\infty}^{\infty} H_y E_z dz)$ for TM-modes, with c being the speed of light in vacuum. The coefficients C_1 and C_2 in Eq. (3) are determined as:

$$C_1 = \frac{\delta p - h_1 \tan h_1 L_1 - \beta v}{\delta p \tan h_1 L_1 + h_1 - \beta v \tan h_1 L_1}, \quad C_2 = \frac{h_2 \tan h_2 L_2 - \sigma q}{h_2 + \sigma q \tan h_2 L_2} \tag{4}$$

and the transverse components of the wave vector in each layer are defined as: $h_1^2 = k_0^2 \varepsilon_1 \mu_\perp - \beta^2$ and $h_2^2 = k_0^2 \varepsilon_{yy} \mu_2 - \beta^2$ for TE-modes, $h_1^2 = k_0^2 \mu_1 \varepsilon_\perp - \beta^2$ and $h_2^2 = k_0^2 \varepsilon_{xx} \mu_2 - (\varepsilon_{xx}/\varepsilon_{zz})\beta^2$ for TM-modes, and $p^2 = \beta^2 - k_0^2 \varepsilon_3$ and $q^2 = \beta^2 - k_0^2 \varepsilon_4$ for the substrate and cladding, respectively. Here $k_0 = \omega/c$ is the wave vector of the electromagnetic wave in air, $\sigma = \mu_2/\mu_4$, $\tau = \mu_1/\mu_2$, $\delta = \mu_1/\mu_3$, $v = \mu_a/\mu_1$ for TE-mode, and $\sigma = \varepsilon_{zz}/\varepsilon_4$, $\tau = \varepsilon_1/\varepsilon_{zz}$, $\delta = \varepsilon_1/\varepsilon_3$, $v = \varepsilon_a/\varepsilon_1$ for TM-mode, with $\mu_\perp = \mu_1 - \mu_a^2/\mu_1$ and $\varepsilon_\perp = \varepsilon_1 - \varepsilon_a^2/\varepsilon_1$ being the transverse permeability and permittivity of the YIG layer, respectively. The dispersion equation, obtained from the boundary conditions, can be written as (Panyaev et al. 2016)

$$\begin{aligned} &\left[\delta\tau p h_2^2 + \sigma q h_1^2 + \beta v(\beta v \sigma q - \delta \sigma p q - \tau h_2^2)\right] \tan h_1 L_1 \cdot \tan h_2 L_2 \\ &+ h_2 \left[h_1^2 - \delta\sigma\tau p q + \beta v(\beta v + \tau\sigma q - \delta p)\right] \tan h_1 L_1 \\ &+ h_1 (\tau h_2^2 - \delta\sigma p q) \tan h_2 L_2 - h_1 h_2 (\delta p + \sigma\, \tau\, q) = 0\ . \end{aligned} \tag{5}$$

If $L_2 = 0$, the Eq. (5) transforms into a conventional dispersion relation for a three-layer waveguide structure (Adams 1981; Barnoski 1974).

The mode order is defined as the number of nodes of the profile function distribution within the waveguide which can be obtained from the condition $F(z) \to 0$. In order to fulfill this condition, the profile functions in the waveguide layers can be written as:

$$\begin{cases} F(-L_1 \le z \le 0) = A \cdot \text{sign}(C_1)\sqrt{1+C_1^2}\sin(h_1 z + \varphi_1), \\ F(0 \le z \le L_2) = A \cdot \text{sign}(C_2)\sqrt{1+C_2^2}\sin(h_2 z + \varphi_2), \end{cases} \tag{6}$$

where $\varphi_1 = \arctan(1/C_1)$ and $\varphi_2 = \arctan(1/C_2)$ are the initial phases. Then the number of nodes in the given layer is:

$$\begin{cases} M_i = \{h_i L_i/\pi\}_{\text{int}} + 1, & \text{if } |\pi \cdot \{h_i L_i/\pi\}_{\text{int}} - h_i L_i| \ge |\varphi_i| \ge 0, \\ M_i = \{h_i L_i/\pi\}_{\text{int}}, & \text{in all other cases.} \end{cases} \tag{7}$$

The subscript $i = 1, 2$ denotes the YIG and NC layers, respectively. The order of the mode is then determined as $M = M_1 + M_2$. Note that for the case of improper modes in open waveguides the above conditions $F(z) \to 0$ for $z \to \pm\infty$) are not valid, because the dispersion equations in such structures have additional complex roots (Manenkov 2009).

3 Numerical results and discussion

For the numerical analysis of the results obtained above, we take into account the dispersion of refractive indices (the Sellmeier equations) of YIG, SiO_2, and GGG:

$$n^2 = 1 + \frac{A_1\lambda^2}{\lambda^2 - B_1^2} + \frac{A_2\lambda^2}{\lambda^2 - B_2^2} + \frac{A_3\lambda^2}{\lambda^2 - B_3^2}, \tag{8}$$

where λ is in microns. Sellmeier coefficients for materials constituting the considered structure are gives in Table 1.

The dispersion of TiO_2 is given as $n^2_{TiO_2} = 5.913 + \frac{0.2441}{\lambda^2 - 0.0803}$ (Devore 1951).

Figure 2a illustrates the dispersion of the refractive indices of the materials constituting the structure under consideration, calculated using the Sellmeier's equations within the range $\lambda = (1 \div 6)\mu$m. For GGG, TiO_2 and SiO_2 layers the dielectric permittivities are: $\varepsilon_{\text{GGG}}(\lambda) = n^2_{\text{GGG}}(\lambda)$, $\varepsilon_{\text{TiO}_2}(\lambda) = n^2_{\text{TiO}_2}(\lambda)$, respectively. The diagonal components of the dielectric permittivity tensor $\hat{\varepsilon}_{\text{YIG}}$ are assumed to be $\varepsilon_1 = n^2_{\text{YIG}}(\lambda)$ and those of the magnetic permeability tensor $\hat{\mu}_{\text{YIG}}$ can be taken as $\mu_1 = 1$ for the considered frequency regime (Gurevich and Melkov 1996). The values of the off-diagonal material tensor components for YIG are defined (Torfeh and Le Gall 1981) with the following MO coefficients: $\varepsilon_a = -2.47 \times 10^{-4}$ and $\mu_a = 8.76 \times 10^{-5}$ [see Eq. (1)].

Figure 2b shows the refractive indices of the NC multilayer and YIG film obtained from the wave localization conditions $h_1 = 0$ and $h_2 = 0$. These conditions confine the

Table 1 Sellmeier coefficients for YIG, GGG and SiO_2

Material	A_1	A_2	A_3	B_1 (μm)	B_2 (μm)	B_3 (μm)
YIG (Johnson and Walton 1965)	3.739	0.79	–	0.28	10	–
GGG (Wood and Nassau 1990)	1.7727	0.9767	4.9668	0.1567	0.01375	22.715
SiO_2 (Malitson 1965)	0.6961663	0.4079426	0.8974794	0.0684043	0.1162414	9.896161

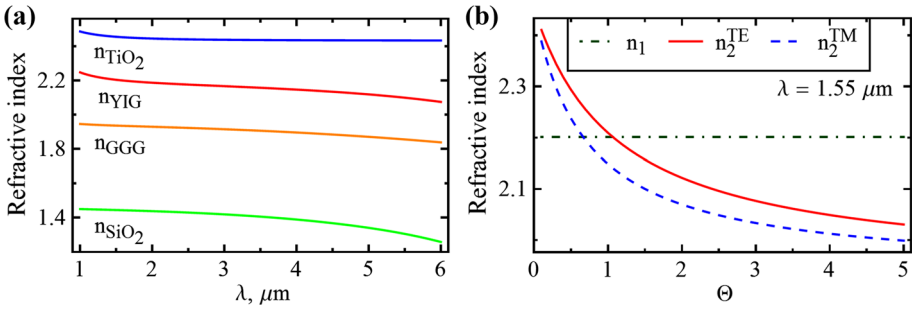

Fig. 2 **a** Refractive indices dispersion $n(\lambda)$ for TiO_2, YIG, GGG and SiO_2; **b** the refractive indices of the NC $n_2^{TE} = \sqrt{\varepsilon_{yy}\mu_2}$ and $n_2^{TM} = \sqrt{\varepsilon_{zz}\mu_2}$ as functions of the ratio Θ between thicknesses of GGG and TiO_2 layers

waveguide propagation of the electromagnetic wave within either the YIG or the NC layer. Thus, one can introduce two propagation regimes: A-regime, in which the waveguide modes are guided by both YIG and NC layers, and B-regime for the modes guided by only one of these layers (Adams 1981). For the NC multilayer, the refractive indices for TE-modes $n_2^{TE} = \sqrt{\varepsilon_{yy}\mu_2}$ and TM-modes $n_2^{TM} = \sqrt{\varepsilon_{zz}\mu_2}$ considerably differ ($n_2^{TE} > n_2^{TM}$), that is a consequence of its optical anisotropy, which, in turn, is due to the nanostructuring of the NC multilayer. The optical anisotropy of YIG, caused by its bigyrotropy, is much smaller, and in this connection its refractive indices n_1^{TE} and n_1^{TM} are almost equal in the considered wavelength range ($n_1^{TE} \cong n_1^{TM} \equiv n_1 = \sqrt{\varepsilon_1\mu_1}$). The differences between n_2^{TE}, n_2^{TM} and n_1 vary with the ratio Θ between thicknesses of GGG and TiO_2 layers, thus selecting the value of Θ, one can set the appropriate waveguide regime for the chosen wavelength.

In Fig. 3 we present the effective refractive index (i.e. normalized wave number β/k_0) (Fig. 3a) and transverse component of the wave vector in NC layer (Fig. 3b) for TE- (red lines) and TM- modes (blue lines) versus normalized frequency $\frac{\omega L_2}{c} = k_0 L_2$. The values of $k_0 L_2$ correspond to the wavelength range $\lambda = (1 \div 6)$ μm. Each dispersion curve is

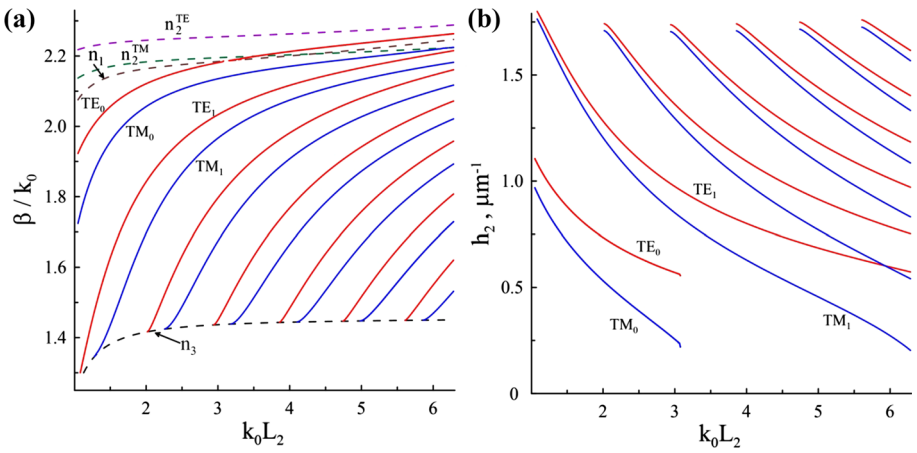

Fig. 3 The normalized wave number β/k_0 (**a**) and wave vector transverse component in the NC layer (**b**) versus the reduced frequency $k_0 L_2$ for the TE- and TM-modes in the four-layer NC structure. The calculations are carried out for $L_1 = L_2 = 1$μm and $\Theta = 0.65$

characterized by the corresponding mode number $M = 0, 1, \ldots$. From Fig. 3a it can be observed, that the part of the TE_0-mode dispersion curve is located below n_1 ($k_0 L_2 < 3$) and corresponds to the A-regime, while the other part is located above n_1 ($k_0 L_2 > 3$) and corresponds to the B-regime of the waveguide propagation in the NC-layer. The dispersion curve of the SiO_2 substrate n_3(the black dashed line) limits TE- and TM-modes from below, while the curve n_2^{TE}(magenta dashed line) limits the modes from above. Note that $n_2^{TE} > n_2^{TM}$ throughout the entire considered wavelength range, as follows from the form of the NC permittivity tensor components and the permittivities of its constituent materials. Figure 3b allows to define the maximal thicknesses of nanolayers in the NC. In fact, we can use the aforementioned inequality which reads now as $d_{TiO_2} \ll 1/h_2$. From Fig. 3b one can estimate that the maximal thickness of a nanolayer d_{TiO_2} is about 50 nm, so that the effective medium approach is still valid. It is worth mentioning that the cutoff regime does not take place for the fundamental modes within the chosen region of $k_0 L_2$.

In Fig. 4 the parameters L_1, L_2 and Θ are chosen so that the dispersion curves n_2^{TM} and n_1 intersect near $\lambda = 1.5\mu m$. Thus from Fig. 4a one can see that the TM_0-mode transforms from the mode, guided by the layer 2 (orange line), to the mode, guided by the layer 1 (cyan line), passing through the area, where it propagates in the A-regime being guided by both layers (blue line). The peak of its Poynting's vector longitudinal component $S_x = -\frac{c}{8\pi}\mathrm{Re}\,(H_y^* E_z)$ shifts from the YIG-layer to the NC with the increase of λ (Fig. 4b). For the

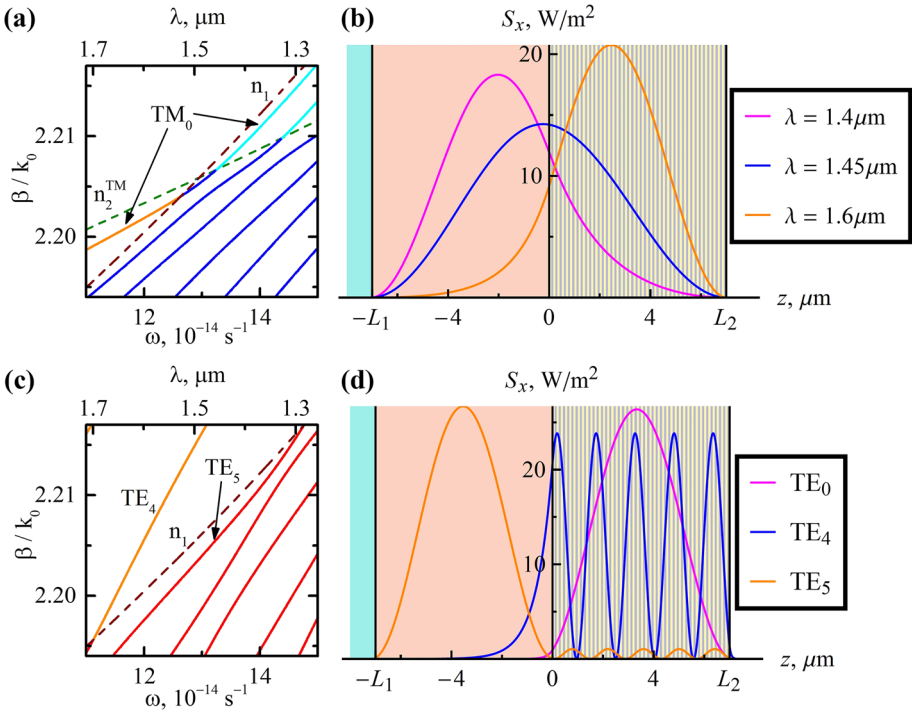

Fig. 4 The spectra of TM- (**a**) and TE-modes (**c**) (normalized wave number β/k_0 vs angular frequency ω and wavelength λ) for the four-layer NC structure. The distribution of the longitudinal Poynting's vector component within the waveguide layers for the fundamental TM_0-mode (**b**) and for TE-modes (**d**) for $\lambda =$ 1.5 μm. The calculations are carried out for $L_1 = L_2 = 7\mu m$ and $\Theta = 0.65$

TE-polarization in this case the dispersion curve n_2^{TE} lies higher, outside the depicted range of β/k_0, and several modes with the mode order up to $M = 4$ propagate in the B-regime in the NC-layer and, all the higher order TE-modes starting from the TE_5-mode are modes of the A-regime, as shown in Figs. 4c, d.

4 Power flux analysis

In Fig. 5 the normalized partial power flux distributions ($P_1 = \int_{-L_1}^{0} S_x dz/P$ in the YIG-layer and $P_2 = \int_{0}^{L_2} S_x dz/P$ in the NC-layer) of the TE- and TM-modes are demonstrated within the fixed region of λ. The total power flux in the structure is $P = \int_{-\infty}^{\infty} S_x dz$. The partial power fluxes of the higher order modes (in contrast to the fundamental modes TE_0 and TM_0) oscillate with the change of λ. The oscillations are more frequent and are less pronounced with the increase of the mode's order M. An appropriate choice of Θ allows to tune the guiding properties of the structure according to the preferable ones. Namely, we can choose a region nearby the telecommunication wavelengths $\lambda \approx 1.3$ μm for TE-modes and $\lambda \approx 1.5$ μm for TM-modes where the equal power flux redistribution between the two waveguide layers takes place. A precise value of Θ for the equal flux redistribution can be obtained from the condition $n_1^{TE}(\Theta) = n_2^{TE}(\Theta)$ or $n_1^{TM}(\Theta) = n_2^{TM}(\Theta)$ for the corresponding orthogonal polarization.

The dependencies of the partial power fluxes vs wavelength for TE_0- and TM_0-modes are plotted in Fig. 6. The calculations are carried out for the symmetric structure with $L_1 = L_2 = 7$μm. The drastic difference between the fluxes of TE_0- and TM_0-modes results to the fact that at the short wavelength one can see a two-channel polarization splitting, i.e. the TE_0-mode propagates in YIG-layer and the TM_0-mode propagates in NC (yellow shaded area in Fig. 6). In the central interval of λ the fundamental TM_0-mode has the logarithmic power switching ratio $\eta = 10\log_{10}(P_1/P_2)$ of the order of 6 dB, which can be achieved in the wavelength range of about 150 nm, where there is no switching for the

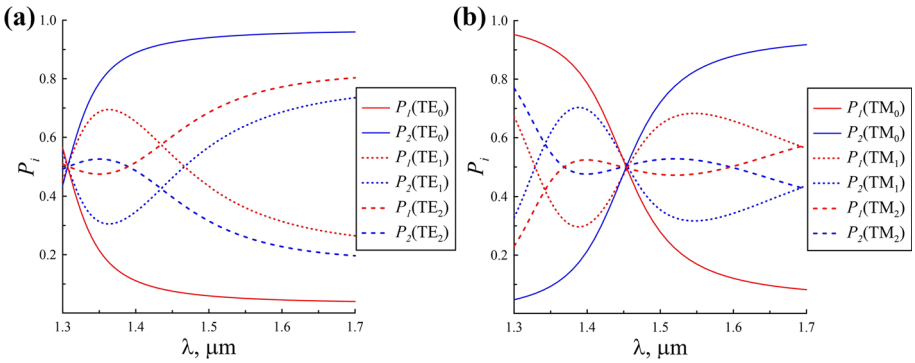

Fig. 5 The guiding modes partial power fluxes P_i as a function of the wavelength λ (the subscripts $i = 1, 2$ denote the YIG and NC layers, respectively) for $L_1 = L_2 = 7$ μm, **a** $\Theta = 1.01$ for TE-modes and **b** $\Theta = 0.65$ for TM-modes

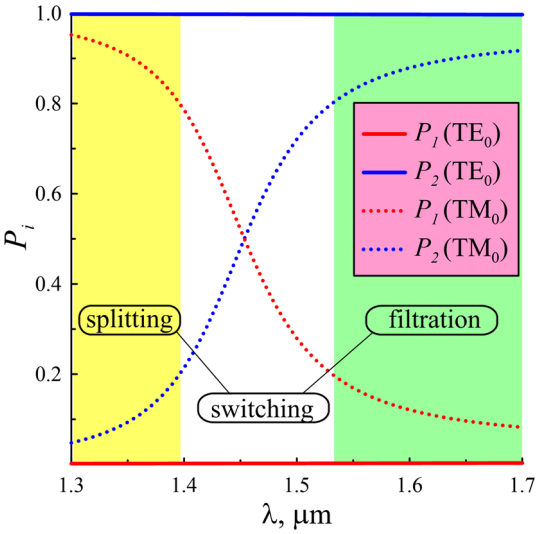

Fig. 6 The partial power fluxes of the fundamental modes P_i as function of the wavelength λ. The calculations are carried out for $L_1 = L_2 = 7\mu m$ and $\Theta = 0.65$. The shaded areas denote the range of the splitting regime (TE_0-mode is localized in NC layer while TM_0-mode is in YIG layer) and filtration regime (TE_0- and TM_0-modes are in NC layer)

TE_0-mode. On the other hand, at the long wavelengths a filtration regime can be realized (green shaded area in Fig. 6), because the partial power fluxes P_1 are small, so the TE_0- and TM_0-modes both propagate in the NC layer.

Hence, the distribution of the power flux across the structure demonstrates the ability either to spatially separate the different polarization modes within the structure or to allocate the main part of the power flux of the fundamental mode between the waveguide layers. In addition, a wavelength-tunable optical switch with the possibility of changing the logical state of the waveguide optical cell can be constructed on the base of the considered structure.

5 Conclusion

Our studies expand and develop our previous investigation (Panyaev et al. 2016) and yield a better understanding of the light control principles in the four-layer structure based on magneto-optical waveguide and nanocomposite-multilayer. This work demonstrates that the optical properties of the guided modes of similar structures can be explicitly analyzed in the framework of long-wave approximation. For instance, we have found the conditions when the TM_0-mode guided by the nanocomposite layer transforms to the mode guided by the magnetic layer, passing through the area, where it is propagating in both layers. We have also shown that the fundamental guided modes (TM_0 and TE_0) can be localized simultaneously in the same layer. Depending on the wavelength, the splitting, switching and filtration propagation regimes can be achieved.

Such a multilayer structure can be used for fabrication of highly efficient optical devices (optical switchers, filters, splitter, etc.) operating in the near- and mid-infrared frequency regimes.

Acknowledgements This research has received funding from the European Union's Horizon 2020 research and innovation program under the Marie Skłodowska-Curie (Grant No. 644348 (N.N.D., Yu.S.D., M.K., and I.L.L.), MPNS COST Action (Project No. MP1403 "Nanoscale Quantum Optics" (N.N.D., Yu.S.D., and

I.L.L.), the Ministry of Education and Science of Russian Federation (Project No. 14.Z50.31.0015 and No. 3.2202.2014/K) (N.N.D., Yu.S.D., I.S.P., and D.G.S.), and Ukrainian State Fund for Fundamental Research (Project No. Ф71/73-2016 "Multifunctional Photonic Structures") (I.L.L.).

References

Adams, M.J.: An Introduction to Optical Waveguides. Wiley, New York (1981)

Agranovich, V.M., Kravtsov, V.E.: Notes on crystal optics of superlattices. Solid State Commun. **55**, 85–90 (1985)

Alaeian, H., Dionne, J.A.: Non-Hermitian nanophotonic and plasmonic waveguides. Phys. Rev. B. **89**, 1–9 (2014)

Barnoski, M.K.: Introduction to Integrated Optics. Plenum, New York and London (1974)

Brekhovskikh, L.M.: Waves in Layered Media. Academic, New York (1980)

Devore, J.R.: Refractive indices of rutile and sphalerite. J. Opt. Soc. Am. **41**, 416–419 (1951)

Dotsch, H., Bahlmann, N., Zhuromskyy, O., Hammer, M., Wilkens, L., Gerhardt, R., Hertel, P., Popkov, A.F.: Applications of magneto-optical waveguides in integrated optics: review. J. Opt. Soc. Am. B. **22**, 240–253 (2005)

Gurevich, A.G., Melkov, G.A.: Magnetization Oscillations and Waves. CRC, New York (1996)

Haus, J.W. (ed.): Fundamentals and Applications of Nanophotonics, vol. 85. Woodhead Publishing Series in Electronic and Optical Materials, Amsterdam (2016)

Hewak, D.W., Lit, J.W.Y.: Generalized dispersion properties of a four-layer thin-film waveguide. Appl. Opt. **26**, 833–841 (1987)

Johnson, B., Walton, A.K.: The infra-red refractive index of garnet ferrites. Br. J. Appl. Phys. **16**, 475–477 (1965)

Khokhlov, N.E., Prokopov, A.R., Shaposhnikov, A.N., Berzhansky, V.N., Kozhaev, M.A., Andreev, S.N., Ravishankar, A.P., Achanta, V.G., Bykov, D.A., Zvezdin, A.K., Belotelov, V.I.: Photonic crystals with plasmonic patterns: novel type of the heterostructures for enhanced magneto-optical activity. J. Phys. D: Appl. Phys. **48**, 095001 (2015)

Khosravi, S., Rostami, A., Rostami, G., Dolatyari, M.: Nanocomposite multilayer structure for broadband MIR negative refractive index. J. Light. Technol. **33**, 4171–4175 (2015)

Kudo, M., Mushiake, Y.: Mode selecting characteristics of four-layer dielectric slab waveguide. Radio Sci. **17**, 125–134 (1982)

Malitson, I.H.: Interspecimen comparison of the refractive index of fused silica. J. Opt. Soc. Am. **55**, 1205–1209 (1965)

Manenkov, A.B.: Propagation of waves in open waveguides with anisotropic dielectrics. Radiophys. Quantum Electron. **24**, 60–69 (1981)

Manenkov, A.B.: Optical waveguide with nonlinear walls. Opt. Quantum Electron. **41**, 169–180 (2009)

Panyaev, I.S., Dadoenkova, N.N., Dadoenkova, Y.S., Rozhleys, I.A., Krawczyk, M., Lyubchanskii, I.L., Sannikov, D.G.: Four-layer nanocomposite structure as an effective optical waveguide switcher for near-IR regime. J. Phys. D: Appl. Phys. **49**, 435103 (2016)

Polky, J.N., Mitchell, G.L.: Metal-clad planar dielectric waveguide for integrated optics. J. Opt. Soc. Am. **64**, 274–279 (1974)

Randoshkin, V.V., Chervonenkis, A.Y.: Applied Magneto-Optics. Energoatomizdat, Moscow (1990). **(in Russian)**

Rao, R., Tang, T.: Study of an active hybrid gap surface plasmon polariton waveguide with nanoscale confinement size and low compensation gain. J. Phys. D: Appl. Phys. **45**, 245101 (2012)

Rytov, S.M.: Electromagnetic properties of a finely stratified medium. Sov. Phys. JETP **2**, 446–475 (1956)

Scifres, D.R., Streifer, W., Burnham, R.D.: Leaky wave room-temperature double heterostructure GaAs: GaAlAs diode laser. Appl. Phys. Lett. **29**, 23–25 (1976)

Smirnova, D.A., Iorsh, I.V., Shadrivov, I.V., Kivshar, Y.S.: Multilayer graphene waveguides. JETP Lett. **99**, 456–460 (2014)

Southwell, W.H.: Index profiles for generalized Luneburg lenses and their use in planar optical waveguides. J. Opt. Soc. Am. **67**, 1010–1014 (1977)

Stiens, J., De Tandt, C., Ranson, W., Vounckx, R., Demeester, P., Moerman, I.: Experimental study of an In0.53Ga0.47As–InP resonant plasma waveguide modulator for medium-infrared light. Appl. Phys. Lett. **65**, 2341–2343 (1994)

Stiens, J., Vounckx, R., Veretennicoff, I., Voronko, A., Shkerdin, G.: Slab plasmon polaritons and waveguide modes in four-layer resonant semiconductor waveguides. J. Appl. Phys. **81**, 1–10 (1997)

Sun, M.J., Muller, M.W.: Measurements on four-layer isotropic waveguides. Appl. Opt. **16**, 814–815 (1977)
Sylgacheva, D.A., Khokhlov, N.E., Kalish, A.N., Belotelov, V.I.: Magnetic control of waveguide modes of Bragg structures. J. Phys.: Conf. Ser. **714**, 12016 (2016a)
Sylgacheva, D., Khokhlov, N., Kalish, A., Dagesyan, S., Prokopov, A., Shaposhnikov, A., Berzhansky, V., Nur-E-Alam, M., Vasiliev, M., Alameh, K., Belotelov, V.: Transverse magnetic field impact on waveguide modes of photonic crystals. Opt. Lett. **41**, 3813–3816 (2016b)
Tabib-Azar, M.: Integrated Optics, Microstructures, and Sensors. Kluwer Academic Publishers, Boston, Dordrecht, and London (1995)
Tien, P.K., Ulrich, R.: Theory of prism-film coupler and thin-film light guides. J. Opt. Soc. Am. **60**, 1325–1337 (1970)
Tien, P.K., Ulrich, R., Martin, R.J.: Modes of propagating light waves in thin deposited semiconductor films. Appl. Phys. Lett. **14**, 291–294 (1969)
Tien, P.K., Smolinsky, G., Martin, R.J.: Thin organosilicon films for integrated optics. Appl. Opt. **11**, 637–642 (1972)
Tien, P.K., Martin, R.J., Smolinsky, G.: Formation of light-guiding interconnections in an integrated optical circuit by composite tapered-film coupling. Appl. Opt. **12**, 1909–1916 (1973)
Torfeh, M., Le Gall, H.: Theoretical analysis of hybrid modes of magnetooptical waveguides. Phys. Status Solidi **63**, 247–258 (1981)
Wood, D.L., Nassau, K.: Optical properties of gadolinium gallium garnet. Appl. Opt. **29**, 3704–3707 (1990)
Yariv, A., Yeh, P.: Optical Waves in Crystals. Wiley, New York (1984)
Yariv, A., Yeh, P.: Photonics: Optical Electronics in Modern Communications. Oxford University, New York and Oxford (2007)
Zvezdin, A.K., Kotov, V.A.: Modern Magnetooptics and Magnetooptical Materials. Institute of Physics, Bristol and Philadelphia (1997)